6-1-2011

Remote Positioning Optical Breast Magnetic Resonance Coil for Slice-Selection During Image-Guided Near-Infrared Spectroscopy of Breast Cancer

Michael A. Mastanduno
Dartmouth College

Shudong Jiang
Dartmouth College

Brian W. Pogue
Dartmouth College

Keith D. Paulsen
Dartmouth College

Roberta DiFlorio-Alexander
Dartmouth College

Remote positioning optical breast magnetic resonance coil for slice-selection during image-guided near-infrared spectroscopy of breast cancer

Michael A. Mastanduno
Shudong Jiang
Roberta DiFlorio-Alexander
Brian W. Pogue
Keith D. Paulsen

Remote positioning optical breast magnetic resonance coil for slice-selection during image-guided near-infrared spectroscopy of breast cancer

Michael A. Mastanduno,[a] **Shudong Jiang,**[a] **Roberta DiFlorio-Alexander,**[b] **Brian W. Pogue,**[a] **and Keith D. Paulsen**[a,b]
[a]Dartmouth College, Thayer School of Engineering, Hanover, New Hampshire 03755
[b]Dartmouth Medical School, Department of Diagnostic Radiology, Lebanon, New Hampshire 03756

Abstract. The design and testing of a pneumatic optical positioning interface produced with the goal of improving fiber positioning in magnetic resonance (MR)-guided diffuse spectral imaging of breast cancer is presented. The system was created for vertical positioning of optical fibers inside the MR bore during a patient exam to target suspicious lesions with MR scans for reference and collect multiple planes of optical data. The interface includes new fiber plates for mechanical and optical coupling to the breast, and was tested in phantoms and human imaging. Reconstructions with data taken in the new interface show acceptable linearity over different absorber concentrations (residual norm = 0.067), and exhibit good contrast recovery at different imaging planes, which is consistent with previous work. An example of human breast imaging through the new interface is shown and a discussion of how it compares to other patient interfaces for breast imaging is presented. Design goals of increasing the available degrees of freedom for fiber positioning while maintaining good patient-fiber contact and comfort were accomplished. This interface allows improved volumetric imaging with interactive and accurate slice selection to quantify targeted suspicious lesions. © *2011 Society of Photo-Optical Instrumentation Engineers (SPIE).* [DOI: 10.1117/1.3587631]

1 Introduction

Image-guided optical spectroscopy is a noninvasive compliment to dynamic contrast enhanced magnetic resonance (MR) imaging (DCE-MRI) of breast cancer that produces functional maps of tissue physiology, and could be used to inform decisions about MR-guided biopsy. In previous studies, a frequency domain optical imaging system was developed to collect amplitude and phase data concurrently with the patient's DCE-MRI exam.[1,2] While the MRI produces a fully three-dimensional (3D) volumetric image stack, the optical system used was inhibited by its ability to collect only one plane of data. An individual imaging plane would therefore have to be selected to intersect the suspected tumor regions.[3] To improve on this issue, we developed a device to interactively reposition the optical fibers within the breast coil and to focus on multiple planes with suspected lesions while still positioned inside the MRI machine. This system increases sensitivity across the complete breast volume and leads to more accurate quantification of the relevant tissue volumes.

There have been a few different approaches to optical breast imaging, with fiber arrangements designed for volumetric imaging and flexibility of sampling using rigidly fixed arrays in planar or circular formats. One planar array was produced at the University of Pennsylvania, with a 9×5 grid of 45 source fibers on one surface of the breast plate for full coverage of the breast volume.[4,5] This group also produced the first MRI-guided near-infrared spectroscopy (NIRS) system, which used a source fiber grid of 8×3 and a detector fiber grid of 4×2 arranged in a contact parallel plate geometry.[6] Schmitz et al created a circular array of up to 25 fiber optics, which were optimized for fast data collection[7] at SUNY Downstate Medical Center. A combined optical imaging and x-ray tomosynthesis system at Massachusetts General Hospital was created with a denser coverage of 40 source fibers in a fixed grid with 9 avalanche photodiode detectors on the opposite side of the breast.[8] Each of these systems take advantage of near-infrared (NIR) imaging's ability to image large tissue volumes through large, accommodating arrays of measurement probes.

More recently, there have been efforts to adapt measurement geometries specifically for each patient through customizable and specific fiber arrays. The SUNY Downstate group designed a dual breast optical tomography system measuring data through up to 31 fibers that completely cover each breast within two semispheres that have adaptable radius. This system can be adjusted for size, tilt, lift, and pitch.[9] Similarly, previous efforts at Dartmouth College used three-layered circular rings of fibers to sample three separate coronal planes through the breast with adjustable radius and coronal position.[10,11] An interface tested at University College London (UCL) consists of interconnected fiber bundle rings mounted to an adjustable conical frame,

Address all correspondence to: Michael Mastanduno, Dartmouth College, Thayer School of Engineering, Hanover, New Hampshire 03755. E-mail: Michael.A.Mastanduno@dartmouth.edu.

allowing construction of custom shapes for each patient breast shape to be imaged. Several efforts in diffuse optical imaging of the brain have also taken advantage of customizable fiber arrangements, such as those at Massachusetts General Hospital[12] and UCL,[13] with elastic or Velcro head caps that are fit to each patient.

In this latest effort reported here for MR-guided optical breast spectroscopy, a pneumatic patient interface was designed and fabricated to allow effective coupling into the MR breast coil as well as accommodate a range of patient breast sizes. This interface is adjustable via computer in the MR control room, allowing for imaging planes to be selected in real-time during a standard DCE-MRI patient exam with the co-registered MRI as a reference. A new fiber plate interface was introduced to provide good optical coupling without problems of transverse light transport through the glass. This report shows the design and test results of this system in tissue-simulating breast phantoms, as well as *in vivo* exams.

2 Materials and Methods

2.1 *Instrumentation*

The MR-NIRS system in this study[1] uses six intensity modulated laser diodes with wavelengths of 660 to 850 nm to illuminate the breast from 16 sequential source positions. The remaining 15 fibers collect transmitted light for detection with photomultiplier tubes (PMTs)(Hamamatsu, 9305–03). The amplitude and phase of the detected light are separated by a lock-in detection method. The imaging system is housed in the MR console room and 12 m fiber bundles are passed through a conduit in the wall to enter the MR scanner room. These fibers are coupled into a custom breast MR coil (Phillips) for simultaneous MR and optical imaging of patients or phantoms. More details on the imaging instrumentation can be found in previous work.[1]

Additional instrumentation has now been implemented to obtain more highly resolved volumetric images. The redesigned optical fiber holder increases the available degrees of freedom for imaging multiple planes in a single patient exam. Since the device is operated from the MR control room, the imaging plane can be adjusted based on the patient's MR image to ensure good coverage of regions of interest. Control from inside the MR computer room is especially important since positioning the tissue in the fiber interface for each exam can displace the anatomical structures. Thus, it is beneficial to use the MR scan to target optimal planes of tissue before optical data acquisition.

Design models and photographs of this interface can be seen in Fig. 1. Two lift bags (Breton Ind., Amsterdam, New York) can be inflated and deflated remotely to raise and lower the imaging plane. A schematic of the control system is also shown in Fig. 1. The air control system utilizes medical air at 50 psi from inside the MR suite, which is controlled to a lower pressure of 5 psi with an adjustable air regulator (Model # R21-03-L00, Wilkerson, Richland, Michigan). Single-acting air solenoid valves (Model # N2-SCD, Mead Fluid Dynamics, Chicago, Illinois) allow or prevent airflow to the lift bags to increase height or remain stationary. Each solenoid valve is electrically connected to a solid-state relay (Model # G3NA210BDC524, Omron, Schaumburg, Illinois) and can be activated by a 5 VDC signal from the system's data acquisition board. A Labview routine controls the height of the imaging arrays separately or simultaneously and provides feedback on the current positions.

Since work by Brooksby et al., we adopted a parallel plane geometry for our MR-guided NIRS system. It is crucial to the newly designed positioning system because the fibers must move but still remain in contact with the breast tissue. Due to the breast's conical shape, a circular fiber array makes this very difficult and a slab geometry is advantageous.
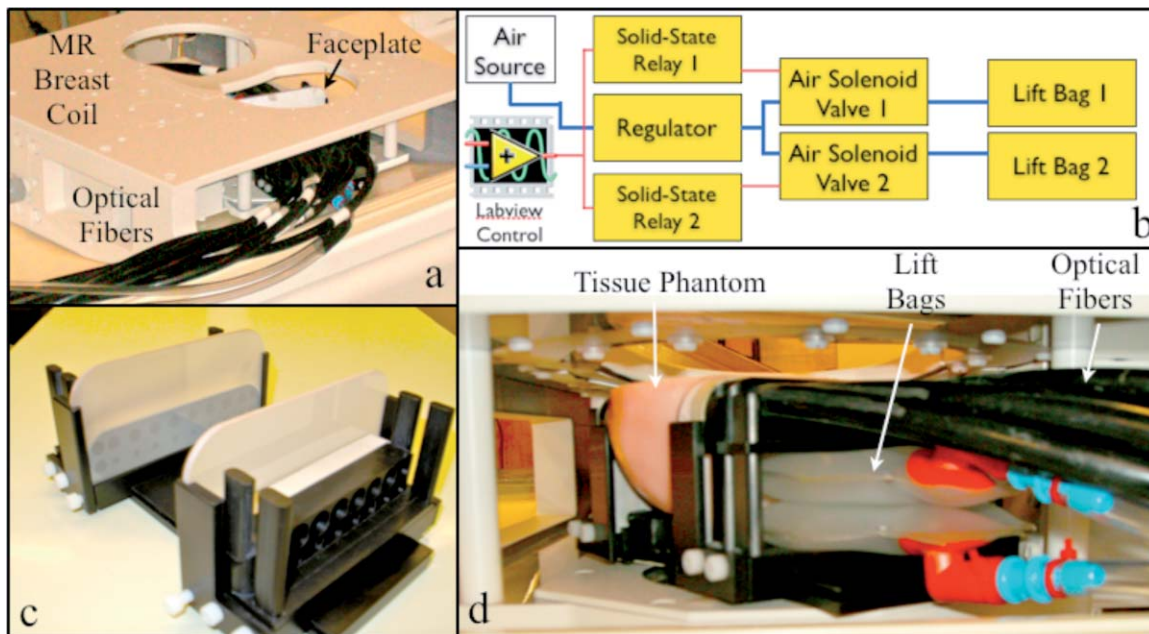

Fig. 1 MR breast coil with MR-optical breast interface integrated (a) and block diagram of control system used to remotely move fibers (b). Photos of interface (c) showing location of the optical fiber-tissue interface (black circles) and (d) in MR breast coil from side with lift bags, optical fibers, and tissue-simulating phantom.

This geometry allowed for more uniform breast shapes, more straightforward patient positioning in the MR, and simplified meshing.

The positioning system was designed with Solidworks software and then machined from black acetal for MR compatibility. It houses optical fiber bundles for the MR-NIRS system and can also hold smaller fibers for simultaneous fluorescence imaging. Nylon set screws rigidly fix the fibers to ensure reliable contact with the imaging domain. Elastic bands provide resistance against the lift bags and lower the device automatically when the lift bags deflate.

The diffusion light propagation model used for spectral image formation requires that the fiber bundles be in reliable contact with the tissue. Thus, we developed a method for keeping these bundles in contact with the breast tissue after placement in the MR coil. This is accomplished with the use of two fiber optics faceplates (Model # 47A, Schott Lighting and Imaging, Southbridge, Massachusetts). This serves as an immobile barrier between the patient and optical fibers. The faceplate acts as a zero-depth window of fused fibers, transferring an undistorted image from one side to the other. The plate's fiber-based constructions have a numerical aperture of 1.0, and remain in rigid contact with the tissue. The source/detector fibers are free to move vertically up and down against the plates, while collecting light emitted from the tissue.

2.2 Image Formation

NIRFAST image reconstruction software minimizes the difference between measured data, and a diffusion-based model for light propagation through tissue.[14–16] The lossy diffusion equation has been well studied in tissue and is an acceptable approximation in regions where scattering (μ_s') dominates over absorption (μ_a) and source-detector separation is greater than a scattering distance.[17] Model data is calculated using the frequency domain diffusion equation [Eq. (1)],

$$-\nabla \cdot D\nabla\Phi(r,\omega) + \left(\mu_a + \frac{i\omega}{c}\right)\Phi(r,\omega) = S(r,\omega) \qquad (1)$$

over finite elements. Here, a source S with frequency ω describes light fluence Φ through the turbid media. We also employ a modified Tikhonov regularization routine with regularization parameter, λ, using a Levenberg-Marquardt style iterative update. This makes the problem less ill-posed, reduces the effects of noise on the image reconstruction, and eliminates improbable solutions.[2] The image formation algorithm [Eq. (2)], is a nonlinear problem which is solved by a Newton-type minimization method:[18]

$$(J^T J + \lambda I)\Delta c = J^T \Delta\delta. \qquad (2)$$

This equation is used to optimize estimation of the physiological parameters c, which includes oxygenated and deoxygenated hemoglobin concentrations, water fraction, scatter amplitude, and scatter power.[19,20] Here, J is the Jacobian matrix, I is the identity matrix, and δ is the model-data misfit. Selection of λ is highly influential on the solutions.[21] It is chosen based on inherent system noise and fiber coupling errors, which are hard to quantify because they are case-specific.[22]

2.3 Phantom Imaging

Two sets of phantom experiments show that data collected with the new interface exhibits linearity and contrast recovery equivalent to previous designs. The first uses a solid resin ink phantom with a hollow cylindrical inclusion.[1] This phantom was placed in the array and the inclusion filled with a 1% Intralipid solution with India ink solution concentrations varying from 0.5% to 4% (made from a stock solution of 0.1% ink in water). Once positioned, this phantom was not moved until after imaging of all concentrations. The lowest ink concentration was used as a calibration data set as described in Ref. 2 to avoid artifacts from index of refraction change between the resin and the liquid inclusion. Though we are capable of measuring these phantoms absolutely, we choose to report relative concentrations. They have proven to be more reliable and are consistent with many other imaging modalities.[23]

The second set of phantoms were constructed from phosphate buffered saline, type 1 Agarose, 1% Intralipid, and whole porcine blood to match the optical properties of normal breast tissue.[24] One phantom had a background hemoglobin concentration of 15 μm, and a 20 mm diameter cylindrical inclusion with $3\times$ hemoglobin contrast and gadolinium MR contrast agent for localization. The other phantom was homogeneous with the same background concentration for calibration purposes.

2.4 Human Subject Imaging

Imaging protocol for the human subject examination was approved by the Committee for the Protection of Human Subjects at Dartmouth–Hitchcock Medical Center. Written consent was obtained prior to imaging. The subjects were positioned into the parallel plate breast interface while on the MR bed by bringing the fiber optics plates into contact with the breast tissue. Some fibers were not in contact with the tissue due to curvature near the edge of the breast. The study used only mild compression as is standard in MR biopsy plates to allow for patient comfort. Co-registration between optical and MR images was done using MR fiducial markers in the plane of the fibers and MR images in the axial geometry. Optical and MR data were collected concurrently, with data collections taking 15 and 45 min, respectively.

3 Results

3.1 System Performance

The fiber positioning system was tested for positioning accuracy and repeatability using pressures from 0.5 to 5.5 psi. Results from the system being repeatedly raised ($n = 10$) are shown in Fig. 2 in a graph of height versus pressure. The array was set up for patient imaging and the computer raised the fibers from bottom to top. A first order fit constrained to go through (0,0) was applied to the data with the norm of the residuals equal to 0.067. Error bars relating to the standard deviation of each measurement are shown and the average standard deviation of all the measurements is 0.23 cm. Due to the system's limited repeatability, precise fiber locations are found using an MR "scout" image and adjusted if necessary after preliminary positioning. Absolute position is most important clinically and can be determined within the resolution limits of MRI.
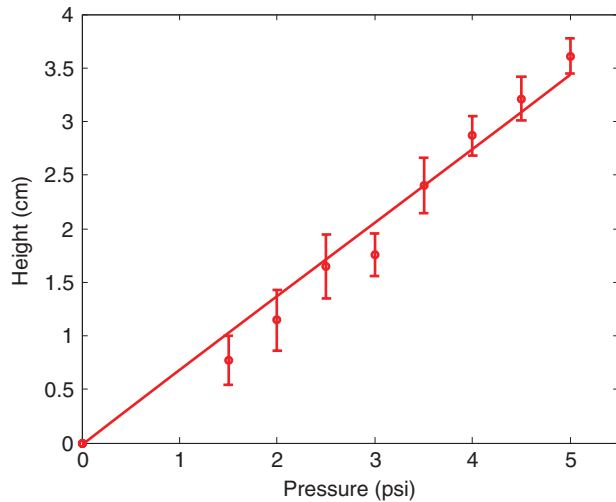
Fig. 2 Fiber height versus system pressure. Height was measured every 0.5 psi from 1.5 psi to 5.0 psi. Error bars show standard deviation at each pressure and a linear fit was applied to the data.

3.2 Solid Phantom Imaging Results

We tested the linearity of the MR-guided NIRS system and multiplanar fiber interface using a resin phantom with dimension of 13.3×5.7 cm with a cylindrical inclusion of radius 1 cm. Using an ink solution concentration of 0.5% for calibration, the phantom was imaged seven times with ink solution concentrations between 1.0% and 4.0%, both with and without the fiber optic plates. 1.0% Intralipid was added to match background scattering. Images were reconstructed on a two-dimensional rectangular finite element mesh with 2577 nodes. Representative single wavelength reconstructions of μ_a and μ_s' are shown in Figs. 3(b) and 3(b), at varying ink concentrations with and without the fiber optic plates. As expected, recovered concentration increased linearly with ink concentration. A 2-region mask with the actual dimensions of the phantom was applied to the

image to separate background and inclusion regions. Nodal values within regions were averaged and their ratio defines recovered contrast. The difference between the plates data and the no plates data is minor and can be seen on the graph of image contrast versus absorber concentration in Fig. 3. A line of best fit to the plates data yields an equation of $0.17x + 0.94$ while the no-plates data yields an equation of $0.17x + 0.98$. Linear fits account for the variance in the data well, with the norm of the residuals being 0.067 and 0.054, respectively. The small difference shows that the fiber plates have a negligible effect on system linearity.

3.3 Gelatin Phantom Imaging Results

The phantoms imaged in the second set were both made from type 1 Agarose with a known 3:1 contrast of whole blood between the background and the inclusion (Fig. 4). The homogeneous phantom that matched the background properties was measured and used for calibration. The inclusion phantom was measured at four different coronal planes using the positioning system to adjust between planes. The exact location of the optical fibers with respect to the inclusion was determined using coronal MR images as a reference.

These data were processed and reconstructed using NIR-FAST with a three-dimensional finite element mesh consisting of 34,211 nodes. Four planes of data were collected and processed using a region-based hard priors approach. Contrast was recorded from each of the four different imaging levels shown on the axial MR image in Fig. 4(c) as well as all of the data together. Absolute optical images of reconstructed HbT are also shown for the data set in Fig. 4 and quantified in Table 1. Though recovered contrast does not reach the true value of 3:1, the dataset with all the planes combined yields image contrast of 2.08:1 with nearly correct inclusion values. The lowest plane has an expectedly low contrast of 1.04:1 and all recovered contrasts are near expected values.
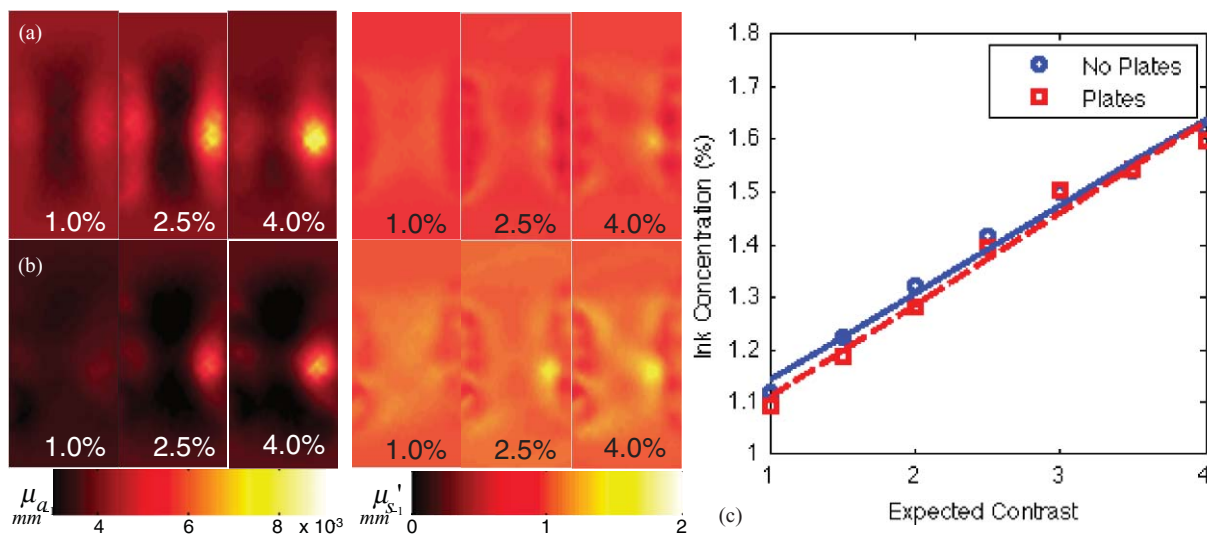

Fig. 3 Images from phantom experiment showing system linearity with (a) and without (b) faceplates. The left block of images quantify μ_a (mm^{-1}) in the domain while the right block shows μ_s' (mm^{-1}). The percentage of ink solution concentration used is written on each image. The graph (c) shows results of linearity over different ink solution concentrations with associated linear regression lines.
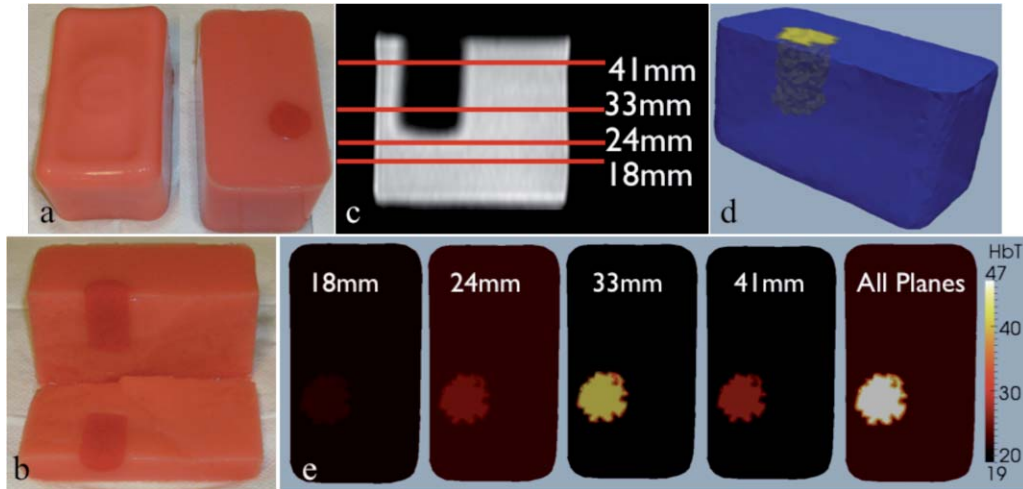
Fig. 4 Phantoms used (a) and (b) in experiment showing contrast recovery. Axial MR image of inclusion phantom (c) with locations of 4 imaging planes shown and text reporting imaging plane distance from bottom of phantom. 3D representation (d) of reconstruction using all 4 data sets simultaneously, and slices (e) through the inclusion after being reconstructed by individual data sets.

3.4 Human Subject Imaging Results

The new interface has been used to successfully image a patient *in vivo* who was undergoing neoadjuvant chemotherapy. Imaging sessions were performed 14 days after the 1st and 2nd cycle of chemotherapy and reconstructed in NIRFAST. The patient was positioned such that her breast was centered in the MR coil to minimize image artifact and then lightly compressed by the fiber optic faceplates. The optical data was collected in approximately 15 min concurrently with the 45 min long MRI exam. After imaging, data from two source/detector fibers was removed because they were not in contact with the breast due to the curvature and would not fit the model.

A 3D finite element mesh consisting of 28,640 nodes was created using Mimics software (Materialise) and region property types were assigned with the help of a radiologist experienced in breast MR. The optical data was co-registered with the MR geometry using MR fiducial markers and reconstructed using a hard priors approach for oxygenated hemoglobin, deoxygenated hemoglobin, water fraction, scatter amplitude, and scatter power. Figure 5 shows a representative axial MR image used for segmentation, along with coronal slices from the reconstructed volume. These solutions were overlaid on corresponding coronal MR images. Axial images show the location of the fiber plane, and optical data was collected in the coronal plane. Fibers were positioned to the optimal location using MRI.

Table 1 Fitted HbT values of background and inclusion in Agarose phantom.

	18 mm	24 mm	33 mm	41 mm	All planes	Truth
Background	21.4	22.8	19.8	18.5	22.6	15.0
Inclusion	22.3	26.8	40.7	27.8	47.0	45.0
Contrast	1.04	1.18	2.05	1.50	2.08	3.0

We found the tumor region to have increases in total hemoglobin, water fraction, and decreases in scattering parameters.

4 Discussion

4.1 Device Development

Imaging the breast using NIRS can be highly dependent on the coupling between optical fibers and breast tissue.[22] The ideal breast coupling interface must be adaptable to many patient sizes, be easily adjustable, and allow for good volumetric sampling—especially close to the chest wall. It must maintain a reliable patient-fiber junction regardless of the position on the breast surface, and be repeatable during different imaging sessions. This current design of the NIRS breast interface is not ideal, but it improves on old iterations in many ways. The most significant improvement is the ability to move vertically with arbitrary slice-selection. Previous designs were mostly limited by their inability to adjust based on MR scans after patient positioning. If the suspected lesion was outside the plane of the fibers, or was displaced after compression, time constraints of the MR exam prevented readjustments. The adjustable pneumatic interface ensures that the most valuable coronal plane is always imaged. Positioning repeatability is limited to ± 2.3 mm, though the exact location can be found using MRI, and fibers can be repositioned if necessary. The fibers can be positioned as close to the chest wall as the MR breast coil will allow, 1.5 cm, and have almost unlimited resolution in step size over an available range of 3.5 cm. Padding is necessary to maintain patient comfort and usually compresses to approximately 1-cm thick. The interface used in previous studies[3,25] is able to get fibers within 2 cm (without padding) of the chest wall over a range of 4.5 cm. The smaller range of 3.5 cm is large enough for almost all cases, and data can be acquired 0.5 cm closer to the chest wall. The breast is held rigidly between the two plates and compressed to uniform, flat sides, which simplifies meshing.

There are shortcomings to the interface as well. We see an approximate 28% loss in light per plate compared to imaging without the plates due to extra index of refraction changes and
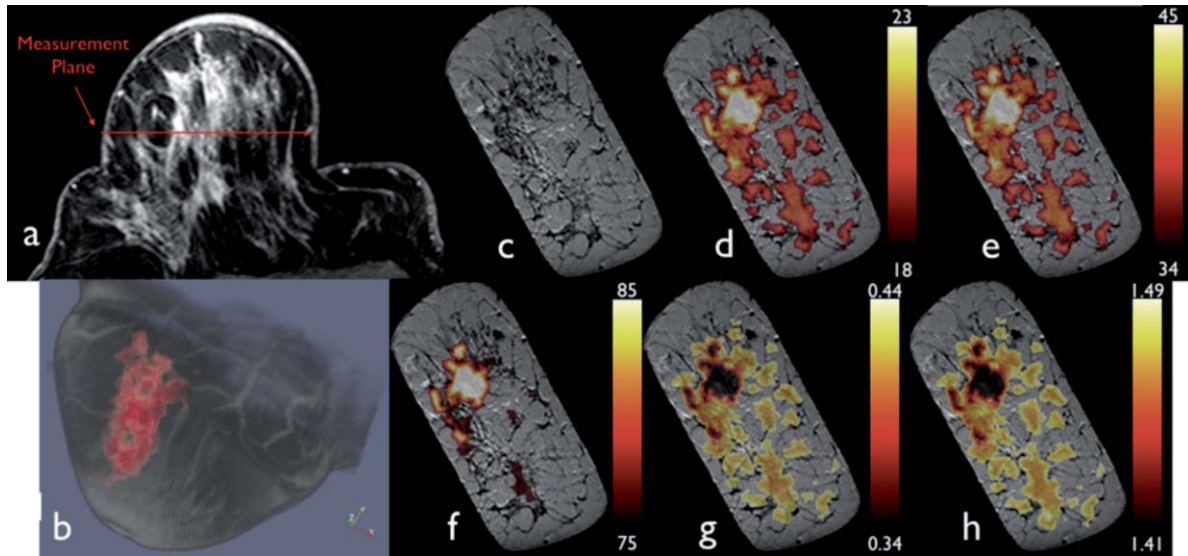
Fig. 5 Illustrative example of patient exam results using MR-optical breast interface. Axial MR imaging showing coronal plane of optical imaging (a). (b) shows a 3D representation of combined maximum intensity projection MR image and 3D rendering of optical solution of HbT. Optical solutions for HbT (d), water (e), oxygen saturation (f), scatter amplitude (g), and scatter power (h), are shown overlaid on top of coronal MR (c). In each case the background value is removed.

cladding between fibers. Since transmission across the breast can produce attenuation of 10 orders of magnitude, the additional loss is not extremely important. The authors attempted to use high quality optical glass instead of fiber face plates but found similar results to Del Bianco et al,[26] where transverse light channeling significantly corrupted reflection mode data. The construction of fiber face plates prevents channeling-related artifacts, justifying the higher cost.

Another problem with the design is that immediate feedback on position is not perfectly accurate. The inherent nonrepeatability of pneumatic systems and the difficulty of measuring air pressure in the MR prevents the computer from knowing exactly where the fibers are positioned at all times. Our accuracy and repeatability test yielded an average standard deviation in positioning of 0.23 cm. Though this is not a negligible amount of uncertainty, we circumvent the problem by using fast scout scans on the MR and looking for fiducial markers that are attached to the fibers. This gives exact positions, but the delay caused to take the scan (usually around 1 min) is still not ideal. Future design iterations will try to improve the accuracy of the interface's position before MR scanning.

4.2 Phantom Interpretation

Validation of new imaging systems can be difficult and usually relies on phantom studies. Though phantoms are not a complete representation of tissue, they are the best way to validate the performance of hardware. Phantoms were made using absorption induced by diluted India ink and scattering from Intralipid, though absolute values of μ_a and μ_s' are still only approximately known for these solutions. Several factors, including batch-to-batch variation, can cause changes in optical properties in phantoms made with these materials from a set recipe. Though it is possible to measure their optical properties, we have found that it is typically more reliable to use relative images.[23] More

importantly, it is not possible to make a phantom that can tailor all imaging parameters to known levels.[27,28] The best option is to use whole blood and evaluate changes in HbT. Even so, this approach does not allow for control of water or scattering parameters exactly. Due to these challenges, we test our instrumentation using linearity over different ink concentrations and contrast recovery at different 2D planes.

The first phantom experiment demonstrates linearity over a range of absorber contrasts with and without the fiber plates in place. The absolute values of the image sets are slightly different, possibly exhibiting crosstalk between absorption and scatter. This could be due to lower light levels from signal loss at the plates' extra index of refraction change. According to these results, the plates do not have a large effect on the recovered image contrast, and large changes from previous patient imaging are not expected.

The second phantom experiment was performed to examine contrast recovery at different planes within a regular volume. As expected, the combined dataset came closest to recovery of the true phantom properties (2.08 versus 3.00) because the additional data create a less ill-posed problem and allow a more accurate reconstruction. The lowest plane is actually homogeneous. It saw little contrast, as only a small portion of the photon path went through the inclusion. The actual contrast recovered was never perfect, likely because the only parameter that varied was blood concentration. Complete contrast recovery is a known problem in diffuse optical tomography[29] that makes contrast imaging more attractive.[23] When looking at HbT values, any crosstalk with other chromophores would decrease the recovered HbT contrast, because it was the only chromophore in the phantom with varying concentration. Water crosstalk also could be an important factor in this experiment because Agarose phantoms have approximately double the water content of breast tissue and our ability to recover water is limited by the PMTs' sensitivity to wavelengths above 850 nm. It has been shown that

longer wavelengths can improve water quantification.[24,28] Thus, it is important to add additional wavelengths to this system. Reconstructed volumes from one plane of data through the new breast MR interface are comparable to past results. As predicted in previous studies,[3,30,31] the combined dataset yields the most accurate quantification due to the larger size and more complete sampling of the volume.

4.3 *Patient Imaging*

Often with human imaging systems, the final and most definitive test is human imaging. An illustrative example of images taken in the new breast MR interface on a patient undergoing neoadjuvant chemotherapy is reported here. This case study demonstrates our ability to position a patient comfortably within the interface, locate the fibers to a desired height, and collect data consistent with previous studies using the same instrument. MRI information was used to accurately position the optical fibers and locate them for optical image formation as shown in the axial MR image [Fig. 5(a)].

With only one patient, it is impossible to interpret the images for prognostic potential. When compared with other patient results of MR and non-MR guided studies,[3,11,25,32] tumor characteristics and data were consistent with other results. More importantly, the interface was successful in imaging the patient from a functional point of view. Difficulty of positioning the interface around the breast tissue was similar to previous designs, yet coverage and flexibly of imaging locations were much improved. The patient did not report any discomfort due to the interface.

5 Conclusions

Since imaging the breast with NIR spectroscopy requires coupling sources and detectors to the breast tissue, image quality and region of interest (ROI) quantification accuracy can be largely dependent on methods used to do so. In this work, the design and testing of a novel, pneumatic optical breast MR interface was shown to improve fiber positioning in MR-guided diffuse optical imaging. Design goals of increasing the available degrees of freedom for fiber positioning while being able to hold the breast rigidly and maintain a reliable patient-fiber interface were accomplished. A system was implemented for repositioning optical fibers from the MR computer room during a patient exam to target suspicious lesions with MR scans as reference and collect multiple planes of data. After basic functionality was achieved, the breast MR optical interface was tested for overall linearity, contrast recovery, and in human imaging. In each case, the results were similar to other studies. As the device has now been validated, future work will concentrate on volumetric imaging and achieving the most accurate quantification of targeted suspicious lesions possible.

References

1. B. Brooksby, S. Jiang, H. Dehghani, B. W. Pogue, K. D. Paulsen, C. Kogel, M. Doyley, J. B. Weaver, and S. P. Poplack, "Magnetic resonance-guided near-infrared tomography of the breast," *Rev. Sci. Instrum.* **75**(12), 5262–5270 (2004).
2. T. O. McBride, B. W. Pogue, S. Jiang, U. L. Osterberg, and K. D. Paulsen, "Development and calibration of a parallel modulated near-infrared tomography system for hemoglobin imaging in vivo," *Rev. Sci. Instrum.* **72**(3), 1817–1824 (2001).
3. C. Carpenter, S. Srinivasan, B. Pogue, and K. Paulsen, "Methodology development for three-dimensional MR-guided near infrared spectroscopy of breast tumors," *Opt. Express* **16**(22), 17903–17914 (2008).
4. J. P. Culver, R. Choe, M. J. Holboke, L. Zubkov, T. Durduran, A. Slemp, V. Ntziachristos, B. Chance, and A. G. Yodh, "Three-dimensional diffuse optical tomography in the parallel plane transmission geometry: evaluation of a hybrid frequency domain/continuous wave clinical system for breast imaging," *Med. Phys.* **30**(2), 235–247 (2003).
5. R. Choe, A. Corlu, K. Lee, T. Durduran, S. D. Konecky, M. Grosicka-Koptyra, S. R. Arridge, B. J. Czerniecki, D. L. Fraker, A. DeMichele, B. Chance, M. A. Rosen, and A. G. Yodh, "Diffuse optical tomography of breast cancer during neoadjuvant chemotherapy: A case study with comparison to MRI," *Med. Phys.* **32**(4), 1128–1139 (2005).
6. V. Ntziachristos, A. G. Yodh, M. D. Schnall, and B. Chance, "MRI-guided diffuse optical spectroscopy of malignant and benign breast lesions," *Neoplasia* **4**(4), 347–354 (2002).
7. C. H. Schmitz, M. Locker, J. M. Lasker, A. H. Hielscher, and R. L. Barbour, "Instrumentation for fast functional optical tomography," *Rev. Sci. Instrum.* **73**(2), 429–439 (2002).
8. A. Li, E. L. Miller, M. E. Kilmer, T. J. Brukilaccio, T. Chaves, J. Stott, Q. Zhang, T. Wu, M. Choriton, R. H. Moore, D. B. Kopans, and D. A. Boas, "Tomographic optical breast imaging guided by three-dimensional mammography," *Appl. Opt.* **42**(25), 5181–5190 (2003).
9. C. H. Schmitz, D. P. Klemer, R. Hardin, M. S. Katz, Y. Pei, H. L. Graber, M. B. Levin, R. D. Levina, N. A. Franco, W. B. Solomon, and R. L. Barbour, "Design and implementation of dynamic near-infrared optical tomographic imaging instrumentation for simultaneous dual-breast measurements," *Appl. Opt.* **44**(11), 2140–2153 (2005).
10. B. W. Pogue, S. Jiang, H. Dehghani, C. Kogel, S. Soho, S. Srinivasan, X. Song, T. D. Tosteson, S. P. Poplack, and K. D. Paulsen, "Characterization of hemoglobin, water, and NIR scattering in breast tissue: analysis of intersubject variability and menstrual cycle changes," *J. Biomed. Opt.* **9**(3), 541–552 (2004).
11. S. Jiang, B. W. Pogue, C. M. Carpenter, S. P. Poplack, W. A. Wells, C. A. Kogel, J. A. Forero, L. S. Muffly, G. N. Schwartz, K. D. Paulsen, and P. A. Kaufman, "Evaluation of breast tumor response to neoadjuvant chemotherapy with tomographic diffuse optical spectroscopy: case studies of tumor region-of-interest changes," *Radiology* **252**(2), 551–560 (2009).
12. M. A. Franceschini, D. K. Joseph, T. J. Huppert, S. G. Diamond, and D. A. Boas, "Diffuse optical imaging of the whole head," *J. Biomed. Opt.* **11**(5), 054007 (2006).
13. H. Dehghani, B. R. White, B. W. Zeff, A. Tizzard, and J. P. Culver, "Depth sensitivity and image reconstruction analysis of dense imaging arrays for mapping brain function with diffuse optical tomography," *Appl. Opt.* **48**(10), D137–143 (2009).
14. H. Dehghani, M. E. Eames, P. K. Yalavarthy, S. C. Davis, S. Srinivasan, C. M. Carpenter, B. W. Pogue, and K. D. Paulsen, "Near infrared optical tomography using NIRFAST: Algorithm for numerical model and image reconstruction," *Commun. Numer. Methods Eng.* **25**(6), 711–732 (2008).
15. H. Dehghani, B. W. Pogue, J. Shudong, B. Brooksby, and K. D. Paulsen, "Three-dimensional optical tomography: resolution in small-object imaging," *Appl. Opt.* **42**(16), 3117–3128 (2003).
16. T. O. McBride, B. W. Pogue, E. Gerety, S. Poplack, U. L. Osterberg, and K. D. Paulsen, "Spectroscopic diffuse optical tomography for quantitatively assessing hemoglobin concentration and oxygenation in tissue," *Appl. Opt.* **38**(25), 5480–5490 (1999).

17. S. R. Arridge and M. Schweiger, "Photon-measurement density functions. Part 2: Finite-element-method calculations," *Appl. Opt.* **34**, 8026–8037 (1995).

18. S. R. Arridge, M. Scheiger, and D. T. Delpy, "Iterative reconstruction of near infrared absorption images," *Proc. SPIE* **1767**, 372–383 (1992).

19. A. Corlu, R. Choe, T. Durduran, K. Lee, M. Schweiger, S. R. Arridge, E. M. Hillman, and A. G. Yodh, "Diffuse optical tomography with spectral constraints and wavelength optimization," *Appl. Opt.* **44**(11), 2082–2093 (2005).

20. S. Srinivasan, B. W. Pogue, B. Brooksby, S. Jiang, H. Dehghani, C. Kogel, W. A. Wells, S. Poplack, and K. D. Paulsen, "Near-infrared characterization of breast tumors in-vivo using spectrally-constrained reconstruction," *Technol. Cancer Res. Treat.* **4**(5), 513–526 (2005).

21. P. K. Yalavarthy, B. W. Pogue, H. Dehghani, and K. D. Paulsen, "Weight-matrix structured regularization provides optical generalized least-squares estimate in diffuse optical tomography," *Med. Phys.* **34**(6), 2085–2098 (2007).

22. M. Schweiger, I. Nissilä, D. A. Boas, and S. R. Arridge, "Image reconstruction in optical tomography in the presence of coupling errors," *Appl. Opt.* **46**(14), 2743–2756 (2007).

23. S. P. Poplack, T. D. Tosteson, W. A. Wells, B. W. Pogue, P. M. Meaney, A. Hartov, C. A. Kogel, S. K. Soho, J. J. Gibson, and K. D. Paulsen, "Electromagnetic breast imaging: Results of a pilot study in women with abnormal mammograms," *Radiology* **243**(2), 350–359 (2007).

24. J. Wang, S. D. Jiang, Z. Z. Li, R. M. diFlorio-Alexander, R. J. Barth, P. A. Kaufman, B. W. Pogue, and K. D. Paulsen, "In vivo quantitative imaging of normal and cancerous breast tissue using broadband diffuse optical tomography," *Med. Phys.* **37**(7), 3715–3724 (2010).

25. C. M. Carpenter, B. W. Pogue, S. Jiang, H. Dehghani, X. Wang, K. D. Paulsen, W. A. Wells, J. Forero, C. Kogel, J. B. Weaver, S. P. Poplack, and P. A. Kaufman, "Image-guided optical spectroscopy provides molecular-specific information in vivo: MRI-guided spectroscopy of breast cancer hemoglobin, water, and scatterer size," *Opt. Lett.* **32**(8), 933–935 (2007).

26. S. Del Bianco, F. Martelli, and G. Zaccanti, "Effect of a clear layer at the surface of a diffusive medium on measurements of transmittance and reflectance," *Opt. Express* **12**(22), 5510–5517 (2004).

27. S. Jiang, B. W. Pogue, T. O. McBride, and K. D. Paulsen, "Quantitative analysis of near-infrared tomography: sensitivity to the tissue-simulating precalibration phantom," *J. Biomed. Opt.* **8**(2), 308–315 (2003).

28. J. Wang, S. C. Davis, S. Srinivasan, S. Jiang, B. W. Pogue, and K. D. Paulsen, "Spectral tomography with diffuse near-infrared light: inclusion of broadband frequency domain spectral data," *J. Biomed. Opt.* **13**(4), 041305 (2008).

29. B. W. Pogue, S. C. Davis, X. Song, B. A. Brooksby, H. Dehghani, and K. D. Paulsen, "Image analysis methods for diffuse optical tomography," *J. Biomed. Opt.* **11**(3), 33001 (2006).

30. H. Dehghani, B. W. Pogue, S. P. Poplack, and K. D. Paulsen, "Multi-wavelength three-dimensional near-infrared tomography of the breast: initial simulation, phantom, and clinical results," *Appl. Opt.* **42**(1), 135–145 (2003).

31. S. Srinivasan, C. Carpenter, and B. W. Pogue, "Sensitivity of hemoglobin concentration on optical probe positioning in image-guided near infrared spectroscopy," in *Ann. Int. Conf. of the IEEE Engineering in Medicine and Biology Society*, Minneapolis, MN, pp. 1994–1996 (2009).

32. S. Srinivasan, B. W. Pogue, S. Jiang, H. Dehghani, C. Kogel, S. Soho, J. J. Gibson, T. D. Tosteson, S. P. Poplack, and K. D. Paulsen, "In vivo hemoglobin and water concentrations, oxygen saturation, and scattering estimates from near-infrared breast tomography using spectral reconstruction1," *Acad. Radiol.* **13**(2), 195–202 (2006).